

OPEN

Realization of efficient quantum gates with a superconducting qubit-qutrit circuit

T. Bækkegaard¹, L. B. Kristensen¹, N. J. S. Loft¹, C. K. Andersen², D. Petrosyan³ & N. T. Zinner^{1,4}

Building a quantum computer is a daunting challenge since it requires good control but also good isolation from the environment to minimize decoherence. It is therefore important to realize quantum gates efficiently, using as few operations as possible, to reduce the amount of required control and operation time and thus improve the quantum state coherence. Here we propose a superconducting circuit for implementing a tunable system consisting of a qutrit coupled to two qubits. This system can efficiently accomplish various quantum information tasks, including generation of entanglement of the two qubits and conditional three-qubit quantum gates, such as the Toffoli and Fredkin gates. Furthermore, the system realizes a conditional geometric gate which may be used for holonomic (non-adiabatic) quantum computing. The efficiency, robustness and universality of the presented circuit makes it a promising candidate to serve as a building block for larger networks capable of performing involved quantum computational tasks.

Richard Feynman famously suggested to simulate quantum physics with quantum computers¹. Fourteen years later, Seth Lloyd proved that an array of spins with tunable interactions indeed represents a universal quantum simulator². Dynamically controlled spin chains can realize analog quantum simulations and digital quantum computations. Several physical systems are being explored for implementing tunable spin chains in the quantum regime, including trapped ions and atoms^{3–5}, quantum dots⁶ and superconducting circuits^{7,8}. Over the last decade, superconducting circuits have steadily improved to become one of the most prominent candidates for the realization of scalable quantum computing^{9–12}. With the development of the transmon qubit¹³ and further advances, such as the 3D transmon¹⁰, coherence times above 44 μs ^{14–17} and per-step multi-qubit gate fidelity at the fault tolerance threshold for surface code error correction¹⁸ have been achieved on multi-qubit devices¹⁹.

Many approaches for entangling quantum gates with superconducting qubits have been implemented experimentally^{19–27} and many more have been proposed theoretically^{28–33}. Still, as the search for better coherence, lower error rates and faster quantum gate operation times continues, more efficient universal realizations of key operations for a quantum processor are needed. Most implementations so far have used only one- and two-qubit quantum operations for realizing important multi-qubit gates³⁴ such as the three-qubit quantum Toffoli³⁵ (CCNOT) and Fredkin³⁶ (CSWAP) gates, requiring a theoretical minimum of five two-qubit gates^{34,37,38}. This large number of required gates can be remedied by the use of a higher-lying state of a qutrit which can simplify the implementation of e.g. the Toffoli gate to three two-qubit gates as implemented optically in³⁹ and in superconducting circuits in⁴⁰. Moreover, the current implementations are highly specialized, meaning that the fabricated superconducting circuit is used just to implement a single three-qubit gate. A single circuit implementing several important universal quantum gates with high fidelity and minimal external control is therefore desirable.

Here, we propose a superconducting circuit realizing two qubits and a qutrit in between. First we show how the circuit can be used to generate two- and three-qubit entangled states^{34,41,42}. Then we discuss how to implement the Fredkin gate using only two three-qubit operations, and the Toffoli gate using two (one-qubit) Hadamard gates and a three-qubit gate employing the intrinsic Ising-like ZZ (longitudinal) couplings and an external one-qubit driving. Finally we discuss how to implement a double-controlled universal unitary single-qubit gate. To illustrate this capability, we use the ZZ-couplings to realize the double-controlled holonomic gate^{43,44}. The geometric nature

¹Department of Physics and Astronomy, Aarhus University, DK-8000, Aarhus C, Denmark. ²Department of Physics, ETH Zürich, CH-8093, Zürich, Switzerland. ³Institute of Electronic Structure and Laser, FORTH, GR-71110, Heraklion, Greece. ⁴Aarhus Institute of Advanced Studies, Aarhus University, DK-8000, Aarhus C, Denmark. Correspondence and requests for materials should be addressed to N.T.Z. (email: zinner@phys.au.dk)

Received: 15 January 2019

Accepted: 8 August 2019

Published online: 16 September 2019

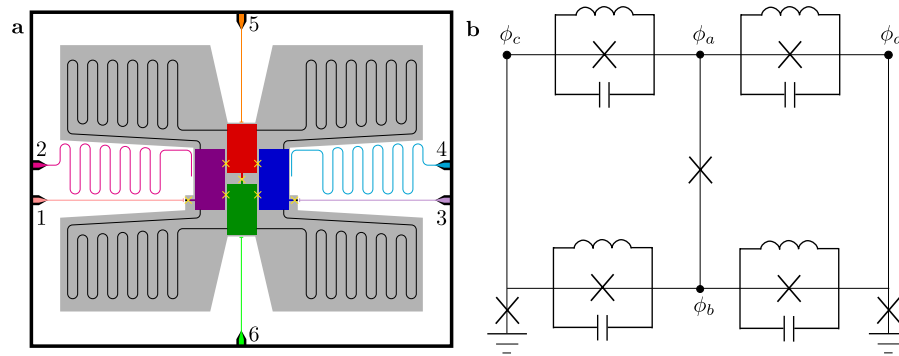


Figure 1. (a) Sketch of a possible physical implementation of the proposed circuit. Each colored box is a superconducting island corresponding to a node in a lumped circuit element model. Josephson junctions are shown schematically as yellow crosses. Bent black wires are inductors. The numbered colored lines are controls for readout and driving of the circuit: 1 and 3 are the flux lines for frequency tuning of the outer qubits, 2 and 4 are resonators capacitively coupled to left and right qubits, and lines 5 and 6 are control and driving of the two middle islands forming the middle qutrit. (b) Effective Lumped circuit scheme of the same circuit. The four nodes in the system are shown as dots and Josephson Junctions are shown as crosses.

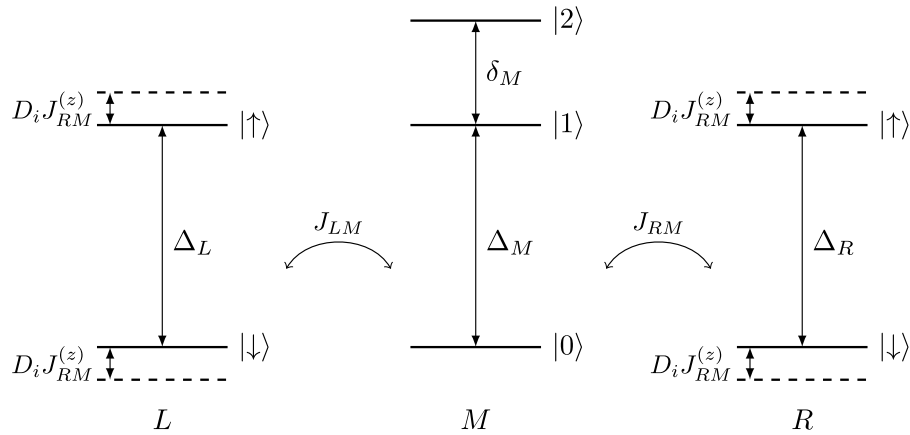


Figure 2. Energy diagram of the system of two qubits (left, L , and right, R) and a qutrit (middle, M) described by the Hamiltonian in Equation (1). Also shown are the exchange couplings $J_{\alpha M}$ and state-dependent energy shifts $J_{\alpha M}^{(z)}$ of (1). D_i depend on the state of the qutrit $|i\rangle$, with, $D_0 = 0$, and typically, $D_1 \gtrsim 2$ and $D_2 \lesssim 4$.

of the holonomic gate provides robustness, but the first proposals required adiabatic control leading to more time for errors to occur. The increase in errors was partly avoided by the introduction of decoherence-free subspaces⁴⁵, which can significantly reduce the detrimental effects of noise. We will instead implement a non-adiabatic generalization⁴⁶, circumventing many of these difficulties. Furthermore, we will show that this double-controlled gate can be used to implement the three-qubit Deutsch gate and is therefore universal for quantum computing in itself, adding yet another tool in our toolbox for efficient quantum gates.

Results

Effective Hamiltonian of the system.

Consider the circuit with four connected superconducting islands and the corresponding effective lumped circuit element model in Fig. 1. The top-bottom symmetry between the capacitors and the Josephson junctions cancels the direct exchange interaction mediated by the capacitances and the leading order term from the Josephson junctions. On the other hand, we choose an asymmetry in the inductive couplings such that the difference between them controls the Heisenberg-like exchange (transverse) coupling, which can be made arbitrarily small if so desired. Furthermore, while the exchange interaction mediated by the leading-order Josephson term ($E_J/2$ in Supplemental Note 1) is canceled by symmetry, the dispersive (ZZ) coupling survives. The couplings are defined in Eq. (A61) and as seen in Supplementary Note 2, a ZZ coupling strength of ~ 20 MHz is realistic. Moreover, the ZZ coupling can be tuned *in-situ* by an external flux.

Using the effective lumped-element circuit of Fig. 1b and following the standard procedure for circuit quantization^{13,47}, we derive the Hamiltonian of the system involving a suitable set of variable for the relevant dipole modes of the circuit, as detailed in the Method and in more details in the Supplementary Note 1. The Hamiltonian of the resulting qubit-qutrit-qubit system shown in Fig. 2 takes the form:

$$\begin{aligned}
H = & \frac{1}{2}\Delta_L\sigma_L^z + \Delta_M|1\rangle\langle 1| + (\Delta_M + \delta_M)|2\rangle\langle 2| + \frac{1}{2}\Delta_R\sigma_R^z \\
& + J_{LM_01}(\sigma_L^-|1\rangle\langle 0| + \sigma_L^+|0\rangle\langle 1|) \\
& + J_{RM_01}(\sigma_R^-|1\rangle\langle 0| + \sigma_R^+|0\rangle\langle 1|) \\
& + J_{LM_12}(\sigma_L^-|2\rangle\langle 1| + \sigma_L^+|1\rangle\langle 2|) \\
& + J_{RM_12}(\sigma_R^-|2\rangle\langle 1| + \sigma_R^+|1\rangle\langle 2|) \\
& + J_{LM}^{(z)}\sigma_L^z(D_1|1\rangle\langle 1| + D_2|2\rangle\langle 2|) \\
& + J_{RM}^{(z)}\sigma_R^z(D_1|1\rangle\langle 1| + D_2|2\rangle\langle 2|),
\end{aligned} \tag{1}$$

where σ_α^+ and σ_α^- are the spin-1/2 raising and lowering operators for the left ($\alpha = L$) and right ($\alpha = R$) qubits, σ_α^z is the Pauli Z operator, and $\Delta_{L,R}$ is the energy differences between the spin-up and spin-down states of the corresponding qubit. The states of the qutrit are denoted by $|j\rangle$ ($j = 0, 1, 2$), Δ_M is the energy of state $|1\rangle$ and $\Delta_M + \delta_M$ is the energy of state $|2\rangle$, making the anharmonicity equal to $\Delta_M - \delta_M$, with the energy of the ground state $|0\rangle$ set to zero. Δ_M and δ_M can be tuned dynamically by an external flux if additional flux lines are added to the circuit, or by an AC-Stark shift stemming from off-resonant microwave driving⁹ using the lines 5 and 6 in Fig. 1(a) (see Supplementary Note 1). We note that the AC-Stark shift is included here for additional dynamical tuning of the circuit but it is not essential for the gate implementations discussed below.

The exchange (XY) coupling strengths between the qubits and the qutrit are given by $J_{\alpha M}$. Typically, the coupling $J_{\alpha M_{12}}$ ($\alpha = L, R$) to the $|1\rangle \leftrightarrow |2\rangle$ transition is stronger than the coupling $J_{\alpha M_{01}}$ to the $|0\rangle \leftrightarrow |1\rangle$ transition by a factor $\sim\sqrt{2}$. The coefficients $J_{\alpha M}^{(z)}$ determine the dispersive (ZZ) interaction between the qubits and the qutrit with $D_1 \gtrsim 2$ and $D_2 \lesssim 4$, with the two parameters converging at 3 as the mixing is increased via the off-resonant driving. For clarity, these parameters are shown in Fig. 2. In a perfectly left-right symmetric circuit, we have $\Delta_L = \Delta_R$ and $J_{LM} = J_{RM}$ for both qutrit transitions which is assumed below unless otherwise stated.

For typical experimental parameters, the coupling strengths J 's are in the range of few to some tenths of MHz, while the energies Δ 's and δ 's are in the 10 GHz range. We choose realistic values of the experimental parameters so as to stay within the transmon regime¹³.

Apart from the intrinsic dynamics of the system, we will employ an external microwave (mw) field of (variable) frequency ω_{mw} to drive the system. Physically, the driving can be applied through resonators 2 and 4 capacitively coupled to the outer qubits, and control lines 5 and 6 capacitively coupled to the qutrit, as shown in Fig. 1(a). The microwave field induces transitions between the qubit and qutrit states as described by the Hamiltonian

$$\begin{aligned}
H_{mw} = & \cos(\omega_{mw}t)(\Omega_L\sigma_L^+ + \Omega_R\sigma_R^+ \\
& + \Omega_1|0\rangle\langle 1| + \Omega_2|1\rangle\langle 2| + \text{H. c.}),
\end{aligned} \tag{2}$$

where Ω 's are the corresponding Rabi frequencies. Moreover, multifrequency pulses generated by an appropriate microwave source and directed to the qutrit via the control lines can be used to dynamically tune the qutrit transitions (see Supplementary Note 1 for the general treatment of transitions of a capacitively coupled qutrit). We note that unlike our qubits and qutrit, in flux qubits optical selection rules may depend on the magnetic flux⁴⁸.

Our system can be used to achieve many quantum information tasks, examples of which are described below. The qutrit can encode a qubit in either states ($|0\rangle, |1\rangle$) or states ($|0\rangle, |2\rangle$). This is solely a matter of convenience and it is straightforward to toggle between these two encodings by applying a π -pulse on the $|1\rangle \leftrightarrow |2\rangle$ transition.

Qutrit dissociation and entangled state preparation. We now discuss how to deterministically prepare entangled states in the setup, which is of great importance for quantum computation and information tasks^{41,49}. In our system, we can employ the qutrit to deterministically prepare an entangled Bell state between the outer qubits $\frac{1}{\sqrt{2}}(|\downarrow\downarrow\rangle + |\uparrow\uparrow\rangle)$, as detailed below.

First, we tune the energy levels of the qutrit to make its two transitions $|0\rangle \leftrightarrow |1\rangle$ and $|1\rangle \leftrightarrow |2\rangle$ non-resonant with the transitions $|\downarrow\rangle \leftrightarrow |\uparrow\rangle$ of the qubits, i.e., we require that $\Delta_M - \Delta_\alpha \gg J_{\alpha M_{01}}$ and $\delta_M - \Delta_\alpha \gg J_{\alpha M_{12}}$. Starting from the ground state $|0\rangle$, we produce the superposition state $\frac{1}{\sqrt{2}}(|0\rangle + |2\rangle)$ of the qutrit by external driving, employing the STIRAP (STImulated Raman Adiabatic Passage) sequence of pulses⁵⁰, as has been also proposed⁵¹ and implemented⁵² in superconducting circuits before. Namely, we drive the transitions $|0\rangle \leftrightarrow |1\rangle$ and $|1\rangle \leftrightarrow |2\rangle$ with resonant mw-pulses of Rabi frequencies Ω_1 and Ω_2 . The Ω_2 pulse precedes the Ω_1 pulse, and we adjust the overlap between the pulses so as to obtain the transfer to state $|2\rangle$ with minimal population of the intermediate state $|1\rangle$. The two pulses are suddenly turned off when their amplitudes are equal, resulting in the desired superposition state. The dynamics of the qutrit under the STIRAP driving is shown in Fig. 3a, with the inset showing the pulse sequence.

Next, the Bell state is obtained as $\frac{1}{\sqrt{2}}(|\downarrow\downarrow\rangle(|0\rangle + |2\rangle) \rightarrow \frac{1}{\sqrt{2}}(|\downarrow\downarrow\rangle + |\uparrow\uparrow\rangle)|0\rangle$ via ‘‘dissociation’’ of the qutrit excitation $|2\rangle$ into two qubit excitations $|\uparrow\uparrow\rangle$. To this end, we set $\Delta_M + \delta_M = \Delta_L + \Delta_R$ and choose $\Delta_M - \Delta_\alpha > J_{\alpha M_{01}}$ via tuning the frequencies of the outer qubits with flux control and the qutrit with the dynamical driving. Note that this condition applies when $J_{\alpha M_{01}} = J_{\alpha M_{12}}$. If the exchange coefficients are different, as is normally the case, the qutrit is moved out of the two-photon resonance by unequal second order level shifts $|J_{\alpha M_{01}}|^2/(\Delta_M - \Delta_\alpha) \neq |J_{\alpha M_{12}}|^2/(\delta_M - \Delta_\alpha)$, which can be compensated for by adjusting Δ_M or δ_M . Making the

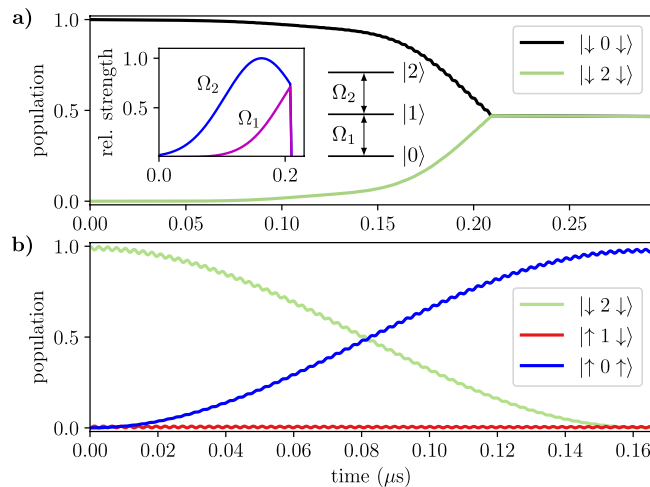


Figure 3. (a) Populations of states $|0\rangle$, $|1\rangle$ and $|2\rangle$ of the middle qutrit during the half STIRAP in the case of off-resonant qutrit levels and $\max(\Omega_{1,2})/2\pi = 20$ MHz. The inset shows the envelopes of the mw pulses. (b) Dissociation of the initial state $|\downarrow 2 \downarrow\rangle$ into the final state $|\uparrow 0 \uparrow\rangle$ with the two-photon resonance $\Delta_M + \delta_M = \Delta_L + \Delta_R$ while the intermediate states $|\uparrow 1 \downarrow\rangle$, $|\downarrow 1 \uparrow\rangle$ are off-resonant. See Supplementary Note 2 for the parameters used in the simulation. We also include finite coherence times as described in Methods.

intermediate state $|1\rangle$ non-resonant precludes its population but prolongs the dissociation, which results in a more pronounced effect of the noise and relaxations. The dissociation dynamics $|\downarrow 2 \downarrow\rangle \rightarrow |\uparrow 0 \uparrow\rangle$ is shown in Fig. 3b.

Using the pairwise ZZ-interactions, the fully entangled three-particle GHZ (Green-Horne-Zeilinger) state $\frac{1}{\sqrt{2}}(|\downarrow 0 \downarrow\rangle + |\uparrow 1 \uparrow\rangle)$ can be obtained from the prepared Bell state $\frac{1}{\sqrt{2}}(|\downarrow 0 \downarrow\rangle + |\uparrow 0 \uparrow\rangle)$ by the external driving of the middle qutrit. To this end, we apply to the circuit a weak π pulse Ω_1 which is resonant only for the $|\uparrow 0 \uparrow\rangle \leftrightarrow |\uparrow 1 \uparrow\rangle$ transition and non-resonant for the $|\downarrow 0 \downarrow\rangle \leftrightarrow |\downarrow 1 \downarrow\rangle$ transition, due to the ZZ interactions with the strengths $J_{\alpha M}^{(z)} \gg \Omega_1$.

Alternatively, we can encode a qubit in the $(|0\rangle, |2\rangle)$ states of the qutrit and produce a different maximally entangled state $\frac{1}{\sqrt{2}}(|\downarrow 2 \downarrow\rangle + |\uparrow 0 \uparrow\rangle)$, equivalent to the GHZ state above. Starting from the simple initial state $|\downarrow 2 \downarrow\rangle$, we use only the intrinsic system dynamics by tuning the parameters until $\Delta_L = \Delta_R = \Delta_M = \delta_M$ and $D_2 J_{\alpha M}^{(z)} = \frac{2\sqrt{6}J_{\alpha M 01}}{\sqrt{(n\pi/c_n)^2 - 1}}$ for $n = 1, 2, 3, \dots$ and $c_n = \cos^{-1}\left(\frac{(-1)^{n+1}}{8}\right)$. Here, n is a parameter controlling at which oscillation between the states $|\downarrow 2 \downarrow\rangle$ and $|\uparrow 0 \uparrow\rangle$ their equal superposition is obtained (lower n is quicker). The disadvantage of this scheme is that it requires very precise tuning of the interactions $J_{\alpha M}^{(z)}$. In contrast, for the method above, only the frequencies have to be adjusted, which is easier using the dynamical tuning or an equivalent flux tuning. Further details are given in Supplementary Note 3.

Toffoli and CCZ gates. The controlled-controlled NOT (CCNOT) gate, also called the Toffoli gate, is a reversible and universal 3-bit gate for classical computation³⁵. It performs a NOT (bit-flip) operation on the target bit if the two control bits are in state ‘1’, and does nothing otherwise. The Toffoli gate is an important element in many quantum algorithms, such as quantum error correction⁵³ and Shor’s algorithm⁵⁴. It has been implemented in systems ranging from trapped ions⁵⁵ to superconducting circuits⁴⁰, including a proposal for an implementation with static control optimized with machine learning⁵⁶.

We can implement the CCNOT gate with the left qubit and the middle qutrit acting as controls and the right qubit being the target. The state of the right qubit is then inverted only if the left qubit is in the spin up (excited) state $|\uparrow\rangle$ and the qutrit is in the ground state $|0\rangle$. The second control qubit is encoded in the qutrit states $|0\rangle$ and $|2\rangle$. The quantum CCNOT gate is realized by first executing a double-controlled phase (CCZ) gate that shifts the phase of the state $|\uparrow 0 \uparrow\rangle$ by π (sign change) while nothing happens if either of the outer qubits are in the spin down state or if the qutrit is in state $|2\rangle$. The CCNOT can then be obtained by the transformation: $\text{CCNOT} = \mathcal{H} \cdot \text{CCZ} \cdot \mathcal{H}$, where \mathcal{H} is the Hadamard gate that acts on the target qubit R . In practice, the Hadamard gate can be obtained by a $\pi/2$ rotation about the y axis.

The CCZ gate is implemented by choosing suitable parameters such that the transitions between the qubit and qutrit states are non-resonant, while $J_{\alpha M}^{(z)}$ (> 10 MHz) is large. We apply a weak microwave field on the qutrit transition $|\uparrow 0 \uparrow\rangle \leftrightarrow |\uparrow 1 \uparrow\rangle$ with the Rabi frequency $\Omega_1 \ll J_{\alpha M}^{(z)}$. Because of the ZZ interactions, which yield a state-dependent frequency shift of the qutrit, the microwave field frequency can be chosen such that it is resonant only when both outer qubits are in the spin-up state. The microwave 2π -pulse then results in the transformation $|0\rangle \rightarrow i|1\rangle \rightarrow -|0\rangle$ that leads to the double conditional π phase change of (only) the state $|\uparrow 0 \uparrow\rangle$. For simplicity, we have here used a standard square-pulse control. In a real-life implementation, a DRAG pulse⁵⁷ or similar optimized pulses could be used, suppressing leakage to, and phase errors from, other levels and thus further improving the fidelity. In Fig. 4, we show the results of the numerical simulations of the CCZ gate in the Hadamard basis

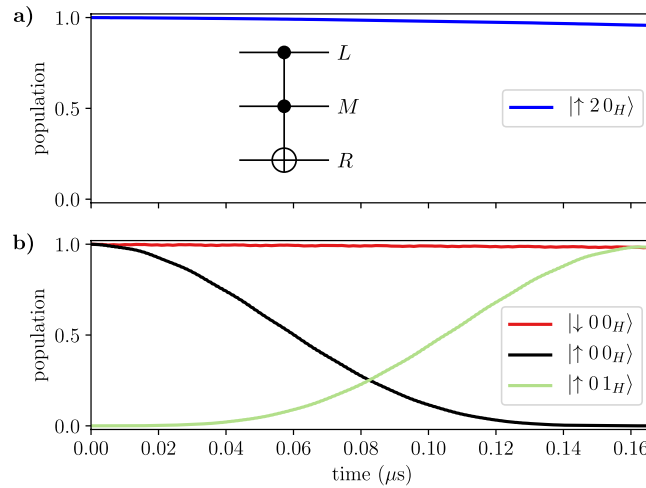


Figure 4. Numerical simulation of the implementation of the ccz gate in the rotating frame. The phase of the right qubit is flipped, $|0_H\rangle \rightarrow |1_H\rangle$, if the left qubit is in state $|\uparrow\rangle$ and the qutrit is in state $|0\rangle$, otherwise no change occurs as exemplified in (a) for the state $|\uparrow 2 0_H\rangle$ and in (b) for the state $|\downarrow 0 0_H\rangle$. A subsequent Hadamard gate on the right qubit will yield the desired CCNOT gate. The standard circuit representation of the Toffoli gate is shown as an inset in the upper panel of the figure. See Supplementary Note 2 for the parameters used in the simulation.

for the right qubit (defined as $|0_H\rangle = |+\rangle = (|\downarrow\rangle + |\uparrow\rangle)/\sqrt{2}$ and $|1_H\rangle = |-\rangle = (|\downarrow\rangle - |\uparrow\rangle)/\sqrt{2}$). Subsequent application of the Hadamard gate to the right qubit will complete the CCNOT gate. We note that because of the symmetry of the driving, we could have also chosen the qutrit state $|1\rangle$ instead of $|0\rangle$ as the ‘open’ state, but here we can view this merely as an ancillary state.

Fredkin gate. Another classically universal 3-bit gate is the Fredkin gate, whose quantum analog is the controlled SWAP (CSWAP) gate. Its effect is to swap the states of the two qubits, $|\uparrow\downarrow\rangle \leftrightarrow |\downarrow\uparrow\rangle$, conditional upon the state of a control qubit, here encoded in the qutrit. We now use the two lowest states ($|0\rangle$ and $|1\rangle$) of the qutrit to encode the qubit such that the excited state $|1\rangle$ is ‘on’ and the ground state $|0\rangle$ is ‘off’. To realize CSWAP, we tune the energy levels of the qutrit such that the transition $|1\rangle \leftrightarrow |2\rangle$ is resonant with the qubit transitions $|\uparrow\rangle \leftrightarrow |\downarrow\rangle$, i.e. $\Delta_L \simeq \delta_M \simeq \Delta_R$. Simultaneously, the qutrit transition $|0\rangle \leftrightarrow |1\rangle$ is largely detuned, $|\Delta_M - \Delta_{L,R}| \gg J_{\alpha M_{01}}$. We then keep the resonance of the exchange interaction $J_{\alpha M_{12}} \gg J_{\alpha M}^{(z)}$ for time $T = \pi/\sqrt{2}J_{\alpha M_{12}}$. If the qutrit is in state $|0\rangle$, the qubits remain in their initial states due to absence of resonant transitions. But if the qutrit is in state $|1\rangle$, it would induce the swap between the qubit states, $|\uparrow\downarrow\rangle \leftrightarrow |\downarrow\uparrow\rangle$, via the resonant intermediate state $|\downarrow 2 \downarrow\rangle$ involving the qutrit excitation. (Resonant swap between the qubits would also occur for the qutrit initially in state $|2\rangle$, with the intermediate state being $|\uparrow 1 \uparrow\rangle$). This is illustrated in Fig. 5a.

As can also be seen in Fig. 5a, however, the initial state $|\downarrow 1 \downarrow\rangle$ has trivial dynamics, unlike the rest of the swapped states which attain a π phase shift during the interaction time T . This means that we have a SWAP operation only up to a conditional phase for an arbitrary superposition input state. This is related to the phase shift of the swapped terms arising in the iSWAP gate, obtained by directly coupling two resonant qubits, which has recently attracted great interest^{9,58}. In our case with the qutrit mediating the swap, only one state has a sign that needs correction, similarly to what Kivlichan *et al.* has recently called the “fermionic simulation gate”⁵⁹. Because of this, we can easily mitigate this problem by using the CCZ gate (see Subsection “Toffoli and CCZ gates”) to attain the π phase shift of state $|\downarrow 1 \downarrow\rangle$ and obtain the correct CSWAP gate. In Fig. 5c we show the results of our numerical simulations of the complete CSWAP protocol, including the conditional resonant SWAP followed by the CCZ gate with a total fidelity $>98\%$. More detailed analysis is given in Supplementary Note 4.

We note that we could have equivalently performed the CSWAP gate between the two qubits via the resonant qutrit transition $|0\rangle \leftrightarrow |1\rangle$, while the other transition $|1\rangle \leftrightarrow |2\rangle$ is non-resonant. In our scheme, the qutrit has to play the role of control and thus our Fredkin gate is not a universal multi-qubit gate in itself. We could, however, imagine another qubit with controlled coupling to the qutrit as part of a larger universal circuit.

Double-controlled holonomic gate. Another concept with importance to quantum computation³⁴ is the implementation of general (non-abelian) one-qubit gates of the form (neglecting overall phase factors)

$$U = \begin{pmatrix} e^{i\phi_1} \cos(\theta) & e^{i\phi_2} \sin(\theta) \\ -e^{-i\phi_2} \sin(\theta) & e^{-i\phi_1} \cos(\theta) \end{pmatrix}. \quad (3)$$

Together with a non-trivial (entangling) multi-qubit gate, they form a universal set of quantum gates³⁴. We can implement the non-adiabatic one-qubit holonomic gate^{44,60} with our qutrit, choosing states ($|0\rangle$, $|2\rangle$) to encode the qubit. Such gates have the advantages of being robust to parameter fluctuations due to the geometric nature,

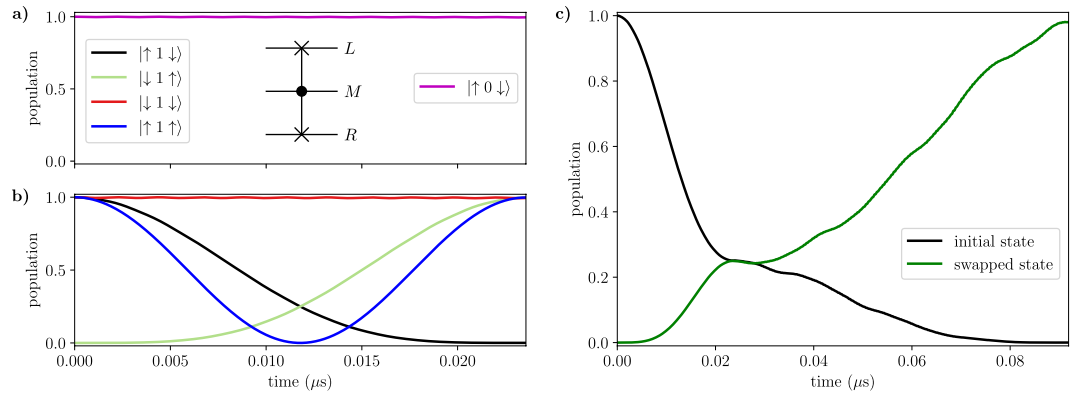


Figure 5. (a and b) Numerical simulations of the ACSWAP (almost CSWAP) gate for different computational basis states, with the exchange interaction $J_{\alpha M_{12}}$ resonant for time $T = \pi/\sqrt{2}J_{\alpha M_{12}}$. The standard circuit representation of the Fredkin gate is shown as an inset in the top part of the figure. (b) Numerical simulation of the full CSWAP gate for the initial superposition state $[\cos(\theta_1)|\uparrow\rangle + e^{i\phi_1}\sin(\theta_1)|\downarrow\rangle]|1\rangle[\cos(\theta_2)|\uparrow\rangle + e^{i\phi_2}\sin(\theta_2)|\downarrow\rangle]$ with $\theta_1 = \pi/4, \phi_1 = 3\pi/4, \theta_2 = 3\pi/4$ and $\phi_2 = \phi_1$. In part 1, we perform the ACSWAP operation during time $T_1 = \pi/2J_{\alpha M_{01}} \simeq 0.025\mu\text{s}$ with the parameters as in panels (a and b). In part 2 we perform the CCZ gate during time $T_2 = 2\pi/\Omega_2$ with the resonant mw field of frequency $\omega_{\text{mw}} = \delta_M - 2J_{\alpha M}^{(z)}$. The full CSWAP fidelity of this state is >0.98 , with finite coherence times included. See Supplementary Note 2 for the parameters used in the simulation.

without the limitations of long gate operation times required to satisfy the adiabatic requirement^{61,62}. Holonomic gates have been implemented in a range of different systems^{63,64}, and their stability has been well tested^{65,66}. Choosing the same system parameters as for the CCZ gate above, we use a driving scheme inspired by⁶³ and thereby realize the single-qubit gate

$$U(\phi, \theta) = \begin{pmatrix} \cos(\theta) & e^{i\phi}\sin(\theta) \\ e^{-i\phi}\sin(\theta) & -\cos(\theta) \end{pmatrix}, \tag{4}$$

with the computational qubit states as basis. This transformation is less general than (3), but it is still universal for one-qubit rotations.

We drive the two transitions $|0\rangle \leftrightarrow |1\rangle$ and $|1\rangle \leftrightarrow |2\rangle$ with the external fields having the same Gaussian envelope $\Omega(t)$ but different complex coupling amplitudes a and b , i.e. $\Omega_1(t) = a\Omega(t)$ and $\Omega_2(t) = b\Omega(t)$ in Equation (2), satisfying $|a|^2 + |b|^2 = 1$. The pulse $\Omega(t)$ is turned on at time $t = 0$ and turned off at $t = \tau$, such that we get a 2π -pulse, $\int_0^\tau \Omega(t)dt = 2\pi$. Notice that this condition ensures that we end up with a closed path in parameter space and the gate is indeed holonomic. Starting with the qutrit in the ground state $|0\rangle$, we then obtain the final transformation $U(\phi, \theta)$ of Equation (4) acting on the qutrit states $|0\rangle, |2\rangle$. Here θ and ϕ are defined via $e^{i\phi}\tan(\theta/2) = a/b$.

By using the $J_{\alpha M}^{(z)}$ couplings to shift the qutrit frequencies, we can make the external driving field resonant or not, depending on the states of the outer qubits. This condition would then result in a controlled-controlled holonomic gate transforming the state of the qutrit according to (4) only when the outer (control) qubits are in e.g. the spin up state. We can show that this new gate is universal for quantum computing by first writing it in the three-qubit computational basis with $|6\rangle = |\uparrow 0 \uparrow\rangle$ and $|7\rangle = |\uparrow 2 \uparrow\rangle$, and the rest of the 8 basis states numbered from 0 to 5:

$$U^c(\phi, \theta) = \begin{pmatrix} \mathbb{I} & 0 \\ 0 & \begin{pmatrix} \cos(\theta) & e^{i\phi}\sin(\theta) \\ e^{-i\phi}\sin(\theta) & -\cos(\theta) \end{pmatrix} \end{pmatrix}, \tag{5}$$

where \mathbb{I} is the 6×6 identity matrix and the superscript c indicates that this is the controlled version of the holonomic gate. We now apply this transformation twice:

$$U^c(\pi/2, \theta)U^c(0, 0) = \begin{pmatrix} \mathbb{I} & 0 \\ 0 & \begin{pmatrix} \cos(\theta) & -i\sin(\theta) \\ -i\sin(\theta) & \cos(\theta) \end{pmatrix} \end{pmatrix}. \tag{6}$$

This is equal to the famous Deutsch gate except for a factor i on the 2×2 rotation matrix. The Deutsch gate is universal for quantum computation⁶⁷, and thus our double-controlled holonomic gate is also universal. Implementation of this gate have previously been proposed using Rydberg atoms⁶⁸, albeit using three laser pulses instead of only two as in our case.

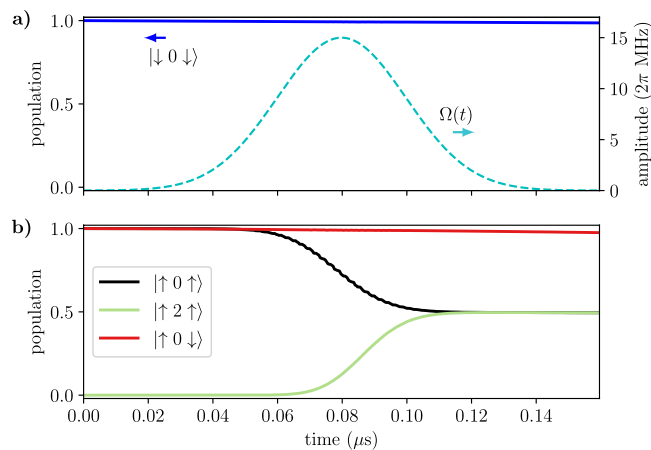


Figure 6. (a and b) Populations (left vertical axes) as function of time during the operation of the controlled-controlled holonomic gate in the case of $\theta = \pi/4$ and $\phi = 0$. Panel (a) also shows the envelope of the external fields plotted with dotted lines with the corresponding vertical axis on the right of the plot. See Supplementary Note 2 for the parameters used in the simulation.

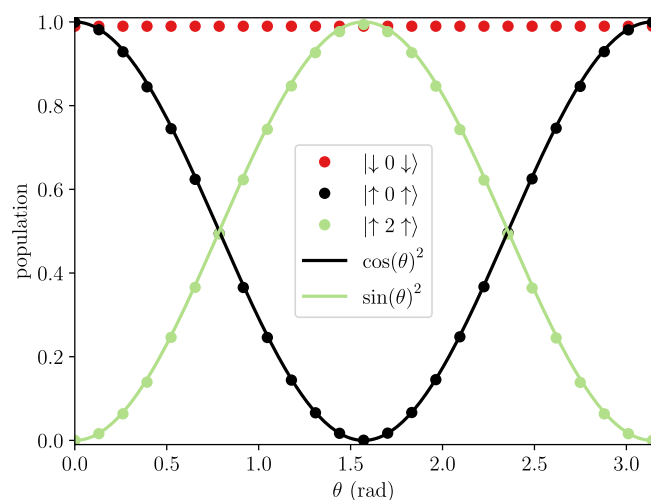


Figure 7. Populations of state versus θ ($\phi = 0$) after the application of the controlled-controlled holonomic gate to the initial state $|\uparrow 0 \uparrow\rangle$ (black and green points) and $|\downarrow 0 \downarrow\rangle$ (red points). See Supplementary Note 2 for the parameters used in the simulation.

In Fig. 6 we show the evolution of different initial states under gate operation. Evidently, the qutrit rotation is blocked when the left qubit is in the spin-down state or both qubits are in the spin down state, while the qutrit is rotated according to Equation (4) when both qubits are in the excited state.

In Fig. 7, we show the populations of the final states for various values of θ , while $\phi = 0$. The theoretical curves $\cos^2\theta$ and $\sin^2\theta$ from (4) are also shown and we observe a very good agreement. The final population of the blocked state $|\downarrow 0 \downarrow\rangle$ is somewhat lower than expected primarily due to leakage to the other levels via a weak interaction with the external field, even though it is far from resonance. This leakage is also apparent in Fig. 6 and can potentially be reduced by employing pulse shaping techniques⁵⁷.

Discussion

To summarize, we have proposed a realistic superconducting circuit, consisting of a qutrit and two qubits, for efficient implementations of multi-qubit quantum gates. By utilizing the second excited state of the qutrit in the middle position, we proposed simple schemes for generating a maximally entangled Bell state of the outer qubits and a GHZ state of the qubits and the qutrit. Furthermore, our construction can implement several important quantum gates, such as the cCNOT (Toffoli), and cSWAP (Fredkin) gates. We note that with qubits only, the theoretically most efficient realizations of the Fredkin and Toffoli gates each requires five two-qubit gates³⁸. State of the art implementations of the Toffoli and CCZ gates using superconducting circuits have operation times ranging from 90 ns (with poor fidelity)⁴⁰ to about 260 ns⁶⁹. As for the Fredkin gate, we are not aware of an implementation with a superconducting circuit, but a hybrid scheme proposal has a gate execution time of 350 ns⁷⁰. Using the

current state of the art superconducting systems requiring 40 ns per two-qubit gate^{71,72}, the total three-qubit gate time would be at least 200 ns. For comparison, our proposed scheme can complete the three-qubit operations in 100 ns. Thus, our results exemplify the flexibility and usefulness of qutrits for very efficient realizations of three-qubit gates, and demonstrate the potential of our circuit to serve as a basis for more complicated superconducting circuits.

Our scheme can implement in principle any controlled-controlled unitary operation on the qutrit. As an example, we have considered the double-controlled non-abelian holonomic quantum gate on a single qubit, which can be used to implement the three-qubit Deutsch gate in only two operations. This implementation is more effective than current proposals with Rydberg atoms⁶⁸, while we are not aware of an implementation using superconducting circuits. We have implemented the holonomic gate as it is robust to parameter noise⁶¹ stemming from the geometric nature of this gate. The strategy of using such gates is known as holonomic quantum computation (HQC)⁴⁴ and the universal non-abelian HQC (NHQC) generalization has since been performed by Sjöqvist *et al.*⁴⁶. Here, three bare energy eigenstates are needed and are conveniently provided by the qutrit. A natural next step is to try to implement the two-qubit non-adiabatic holonomic quantum gate also suggested by Sjöqvist *et al.*, requiring two nearest-neighbor qutrits. Such a gate could be possibly achieved by our circuit upon expanding the basis of one of the outer qubits. Together with the holonomic one-qubit gate, this would realize a universal set of holonomic gates.

Realizing qutrit-qutrit interactions would also open the possibility of implementing higher-order effective spin chains, such as the spin-one Haldane spin model^{73,74}, especially if the coherence times of higher levels are further prolonged⁷⁵.

Another possible use of qutrits and a circuit similar to the one proposed in this paper is the implementation of autonomous quantum error correction via engineered dissipation. With a relatively small increase in circuit complexity including three energy levels, an impressive increase in transmon coherence time was predicted in ref. ⁷⁶.

Methods

Consider the circuit with four connected superconducting islands with lumped element circuit shown in Fig. 1b. After obtaining the Lagrangian of the corresponding effective lumped element model system in the node flux picture, we perform a suitable change of coordinates, primarily mixing the two central flux node coordinates: $\psi_1 = \phi_a + \phi_b - 2\phi_c$, $\psi_2 = \phi_a - \phi_b$ and $\psi_3 = \phi_a + \phi_b - 2\phi_d$, where the ϕ s are the flux node variables shown in the circuit (in natural units). They represent the horizontal dipole mode between the left superconducting island and the two middle islands, the vertical dipole mode between the two middle islands, and the horizontal mode between the right island and the two middle islands, respectively. With this choice of coordinates, we obtain three effective nodes with the relevant degrees of freedom sequentially coupled via non-linear interactions. We truncate the outer nodes to the lowest two states, obtaining qubits, while for the middle node we instead choose to truncate its Hilbert space to the lowest three energy levels, obtaining a qutrit. All three degrees of freedom are in the transmon limit with the kinetic energy terms being much smaller than the potential energy terms. Finally, by transforming to a rotating frame and making a rotating wave approximation to eliminate the fast oscillating terms, we obtain an effective Hamiltonian for the system of two qubits each coupled to the qutrit (see Supplementary Note 1 for the full derivation). This Hamiltonian is given in (1).

The drive line terms are added to the non-truncated Lagrangian as externally varied flux nodes and a transformation to an appropriate frame rotating with the external field is performed. This transformation mixes the variables and after additional rotating wave approximations, the desired external part of the Hamiltonian is obtained along with modifications on the energy parameters, i.e. the AC-Stark shifts, which can be used for tuning the qubits and qutrit in and out of resonance.

We simulate the dissipative dynamics of the system numerically, with the relaxation and decoherence times set to $T_1 = 31 \mu\text{s}$ and $T_2 = 35 \mu\text{s}$ respectively, based on recent studies^{15,75,77} (we use the Python QuTip package⁷⁸, and relaxations are implemented by the simple built-in collapse operator functionality). The parameters of the Hamiltonian used in the numerical simulations are all obtained from realistic experimental circuit parameters, as detailed in Supplementary Note 1, and are listed in Supplementary Note 2 for each implementation.

Data Availability

The data that support the findings of this study are available from N.T.Z. upon request.

References

1. Feynman, R. P. Simulating physics with computers. *International Journal of Theoretical Physics* **21**, 467–488 (1982).
2. Lloyd, S. Universal quantum simulators. *Science* **273**, 1073–1078 (1996).
3. Porras, D. & Cirac, J. I. Effective quantum spin systems with trapped ions. *Phys. Rev. Lett.* **92**, 207901 (2004).
4. Blatt, R. & Roos, C. F. Quantum simulations with trapped ions. *Nature Physics* **8**, 277, review Article (2012).
5. Khajetoorians, A. A., Wiebe, J., Chilian, B. & Wiesendanger, R. Realizing all-spin-based logic operations atom by atom. *Science* **332**, 1062–1064 (2011).
6. Zwanenburg, F. A. *et al.* Silicon quantum electronics. *Rev. Mod. Phys.* **85**, 961–1019 (2013).
7. Blais, A. *et al.* Quantum-information processing with circuit quantum electrodynamics. *Phys. Rev. A* **75**, 032329 (2007).
8. Martinis, J. M., Nam, S., Aumentado, J. & Urbina, C. Rabi oscillations in a large josephson-junction qubit. *Phys. Rev. Lett.* **89**, 117901 (2002).
9. Blais, A., Huang, R.-S., Wallraff, A., Girvin, S. M. & Schoelkopf, R. J. Cavity quantum electrodynamics for superconducting electrical circuits: An architecture for quantum computation. *Phys. Rev. A* **69**, 062320 (2004).
10. Devoret, M. H. & Schoelkopf, R. J. Superconducting circuits for quantum information: An outlook. *Science* **339**, 1169–1174 (2013).
11. Wendin, G. Quantum information processing with superconducting circuits: a review. *Reports on Progress in Physics* **80**, 106001 (2017).
12. Gu, X., Kockum, A. F., Miranowicz, A., Liu, Y. X. & Nori, F. Microwave photonics with superconducting quantum circuits. *Physics Reports* **718–719**, 1–102 (2017).

13. Koch, J. *et al.* Charge-insensitive qubit design derived from the Cooper pair box. *Phys. Rev. A* **76**, 042319 (2007).
14. Barends, R. *et al.* Coherent Josephson qubit suitable for scalable quantum integrated circuits. *Phys. Rev. Lett.* **111**, 080502 (2013).
15. Rigetti, C. *et al.* Superconducting qubit in a waveguide cavity with a coherence time approaching 0.1 ms. *Phys. Rev. B* **86**, 100506 (2012).
16. Kandala, A. *et al.* Hardware-efficient variational quantum eigensolver for small molecules and quantum magnets. *Nature* **549**, 242–246 (2017).
17. Wang, Z. *et al.* Cavity Attenuators for Superconducting Qubits. ArXiv e-prints, arXiv:1807.04849 [quant-ph] (2018).
18. Fowler, A. G., Mariantoni, M., Martinis, J. M. & Cleland, A. N. Surface codes: Towards practical large-scale quantum computation. *Phys. Rev. A* **86**, 032324 (2012).
19. Barends, R. *et al.* Superconducting quantum circuits at the surface code threshold for fault tolerance. *Nature* **508**, 500–503 (2014).
20. Yamamoto, T., Pashkin, Y. A., Astafiev, O., Nakamura, Y. & Tsai, J. S. Demonstration of conditional gate operation using superconducting charge qubits. *Nature* **425**, 941 (2003).
21. DiCarlo, L. *et al.* Demonstration of two-qubit algorithms with a superconducting quantum processor. *Nature* **460**, 240 (2009).
22. Chen, Y. *et al.* Qubit architecture with high coherence and fast tunable coupling. *Phys. Rev. Lett.* **113**, 220502 (2014).
23. McKay, D. C. *et al.* Universal gate for fixed-frequency qubits via a tunable bus. *Phys. Rev. Applied* **6**, 064007 (2016).
24. Song, C. *et al.* 10-qubit entanglement and parallel logic operations with a superconducting circuit. *Phys. Rev. Lett.* **119**, 180511 (2017).
25. Sheldon, S., Magesan, E., Chow, J. M. & Gambetta, J. M. Procedure for systematically tuning up cross-talk in the cross-resonance gate. *Phys. Rev. A* **93**, 060302 (2016).
26. Reagor, M. *et al.* Demonstration of universal parametric entangling gates on a multi-qubit lattice. *Science Advances* **4**, <https://doi.org/10.1126/sciadv.aao3603> (2018).
27. Neeley, M. *et al.* Generation of three-qubit entangled states using superconducting phase qubits. *Nature* **467**, 570 (2010).
28. Wang, X.-B., You, J. Q. & Nori, F. Quantum entanglement via two-qubit quantum Zeno dynamics. *Phys. Rev. A* **77**, 062339 (2008).
29. Romero, G., Ballester, D., Wang, Y. M., Scarani, V. & Solano, E. Ultrafast quantum gates in circuit QED. *Phys. Rev. Lett.* **108**, 120501 (2012).
30. Wang, Y., Zhang, J., Wu, C., You, J. Q. & Romero, G. Holonomic quantum computation in the ultrastrong-coupling regime of circuit QED. *Phys. Rev. A* **94**, 012328 (2016).
31. Puri, S. & Blais, A. High-fidelity resonator-induced phase gate with single-mode squeezing. *Phys. Rev. Lett.* **116**, 180501 (2016).
32. Andersen, C. K. & Mølmer, K. Multifrequency modes in superconducting resonators: Bridging frequency gaps in off-resonant couplings. *Phys. Rev. A* **91**, 023828 (2015).
33. Royer, B., Grimsmo, A. L., Didier, N. & Blais, A. Fast and high-fidelity entangling gate through parametrically modulated longitudinal coupling. *Quantum* **1**, 11 (2017).
34. Nielsen, M. A. & Chuang, I. L. *Quantum Computation and Quantum Information: 10th Anniversary Edition*. (Cambridge University Press, Cambridge, 2010).
35. Toffoli, T. Reversible computing. In *Automata, Languages and Programming: Seventh Colloquium Noordwijkerhout, the Netherlands July 14–18, 1980*, edited by de Bakker, J. & van Leeuwen, J. pp. 632–644 (Springer Berlin Heidelberg, Berlin, Heidelberg, 1980).
36. Fredkin, E. & Toffoli, T. Conservative logic. *International Journal of Theoretical Physics* **21**, 219–253 (1982).
37. Yu, N. & Ying, M. Optimal simulation of Deutsch gates and the Fredkin gate. *Phys. Rev. A* **91**, 032302 (2015).
38. Yu, N., Duan, R. & Ying, M. Five two-qubit gates are necessary for implementing the Toffoli gate. *Phys. Rev. A* **88**, 010304 (2013).
39. Lanyon, B. P. *et al.* Simplifying quantum logic using higher-dimensional Hilbert spaces. *Nature Physics* **5**, 134–140 (2008).
40. Fedorov, A., Steffen, L., Baur, M., da Silva, M. P. & Wallraff, A. Implementation of a toffoli gate with superconducting circuits. *Nature* **481**, 170–172 (2012).
41. Jozsa, R. Entanglement and quantum computation. In *Geometric Issues in the Foundations of Science*, edited by Huggett, S., Mason, L., Tod, K. P., Tsou, S. T. & Woodhouse, N. M. J. (Oxford University Press, Oxford, 1997).
42. DiCarlo, L. *et al.* Preparation and measurement of three-qubit entanglement in a superconducting circuit. *Nature* **467**, 574–578 (2010).
43. Duan, L.-M., Cirac, J. I. & Zoller, P. Geometric manipulation of trapped ions for quantum computation. *Science* **292**, 1695–1697 (2001).
44. Zanardi, P. & Rasetti, M. Holonomic quantum computation. *Physics Letters A* **264**, 94–99 (1999).
45. Wu, L.-A., Zanardi, P. & Lidar, D. A. Holonomic quantum computation in decoherence-free subspaces. *Phys. Rev. Lett.* **95**, 130501 (2005).
46. Sjöqvist, E. *et al.* Non-adiabatic holonomic quantum computation. *New Journal of Physics* **14**, 103035 (2012).
47. Devoret, M. H. Quantum fluctuations in electrical circuits. In *Les Houches, Session LXIII 7.8* (Elsevier Science B.V., Amsterdam, 1997).
48. Liu, Y.-X., You, J. Q., Wei, L. F., Sun, C. P. & Nori, F. Optical selection rules and phase-dependent adiabatic state control in a superconducting quantum circuit. *Phys. Rev. Lett.* **95**, 087001 (2005).
49. DiVincenzo, D. P. The physical implementation of quantum computation. *Fortschritte der Physik* **48**, 771 (2000).
50. Vitanov, N. V., Rangelov, A. A., Shore, B. W. & Bergmann, K. Stimulated Raman adiabatic passage in physics, chemistry and beyond. *Rev. Mod. Phys.* **89**, <https://doi.org/10.1103/RevModPhys.89.015006> (2017).
51. Wei, L. F., Johansson, J. R., Cen, L. X., Ashhab, S. & Nori, F. Controllable coherent population transfers in superconducting qubits for quantum computing. *Phys. Rev. Lett.* **100**, 113601 (2008).
52. Kumar, K. S., Vepsäläinen, A., Danilin, S. & Paraoanu, G. S. Stimulated Raman adiabatic passage in a three-level superconducting circuit. *Nature Communications* **7**, 10628 (2016).
53. Cory, D. G. *et al.* Experimental quantum error correction. *Phys. Rev. Lett.* **81**, 2152–2155 (1998).
54. Shor, P. W. Polynomial-time algorithms for prime factorization and discrete logarithms on a quantum computer. *SIAM Journal on Computing* **26**, 1484–1509 (1997).
55. Monz, T. *et al.* Realization of the quantum Toffoli gate with trapped ions. *Phys. Rev. Lett.* **102**, 040501 (2009).
56. Banchi, L., Pancotti, N. & Bose, S. Quantum gate learning in qubit networks: Toffoli gate without time-dependent control. *npj Quantum Information* **2**, 16019 (2016).
57. Motzoi, F., Gambetta, J. M., Rebentrost, P. & Wilhelm, F. K. Simple pulses for elimination of leakage in weakly nonlinear qubits. *Phys. Rev. Lett.* **103**, 110501 (2009).
58. Roth, M. *et al.* Analysis of a parametrically driven exchange-type gate and a two-photon excitation gate between superconducting qubits. *Phys. Rev. A* **96**, 062323 (2017).
59. Kivlichan, I. D. *et al.* Quantum simulation of electronic structure with linear depth and connectivity. *Phys. Rev. Lett.* **120**, 110501 (2018).
60. Pachos, J. K. *Introduction to Topological Quantum Computation*. 1st ed. (Cambridge University Press, New York, 2012).
61. Solinas, P., Zanardi, P. & Zangh, N. Robustness of non-abelian holonomic quantum gates against parametric noise. *Phys. Rev. A* **70**, 042316 (2004).
62. Pachos, J. & Zanardi, P. quantum holonomies for quantum computing. *International Journal of Modern Physics B* **15**, 1257–1285 (2001).
63. Abdumalikov, A. A. Jr. *et al.* Experimental realization of non-abelian non-adiabatic geometric gates. *Nature* **496**, 482–485 (2013).

64. Feng, G., Xu, G. & Long, G. Experimental realization of nonadiabatic holonomic quantum computation. *Phys. Rev. Lett.* **110**, 190501 (2013).
65. Filipp, S. *et al.* Experimental demonstration of the stability of Berry's phase for a spin-1/2 particle. *Phys. Rev. Lett.* **102**, 030404 (2009).
66. Loredano, J. C., Broome, M. A., Smith, D. H. & White, A. G. Observation of entanglement-dependent two-particle holonomic phase. *Phys. Rev. Lett.* **112**, 143603 (2014).
67. Deutsch, D. Quantum computational networks. *Proceedings of the Royal Society of London A: Mathematical, Physical and Engineering Sciences* **425**, 73–90 (1989).
68. Shi, X.-F. Deutsch, Toffoli, and cnot gates via Rydberg blockade of neutral atoms. *Phys. Rev. Applied* **9**, 051001 (2018).
69. Barnes, E., Arenz, C., Pitchford, A. & Economou, S. E. Fast microwave-driven three-qubit gates for cavity-coupled superconducting qubits. *Phys. Rev. B* **96**, 024504 (2017).
70. Liu, T., Guo, B.-Q., Yu, C.-S. & Zhang, W.-N. One-step implementation of a hybrid fredkin gate with quantum memories and single superconducting qubit in circuit QED and its applications. *Opt. Express* **26**, 4498–4511 (2018).
71. Rol, M. A. *et al.* A fast, low-leakage, high-fidelity two-qubit gate for a programmable superconducting quantum computer. arXiv e-prints, arXiv:1903.02492, arXiv:1903.02492 [quant-ph] (2019).
72. Chow, J. M. *et al.* Universal quantum gate set approaching fault-tolerant thresholds with superconducting qubits. *Phys. Rev. Lett.* **109**, 060501 (2012).
73. Haldane, F. D. M. Nonlinear field theory of large-spin Heisenberg antiferromagnets: Semiclassically quantized solitons of the one-dimensional easy-axis Néel state. *Phys. Rev. Lett.* **50**, 1153–1156 (1983).
74. Affleck, I. Quantum spin chains and the Haldane gap. *Journal of Physics: Condensed Matter* **1**, 3047 (1989).
75. Peterer, M. J. *et al.* Coherence and decay of higher energy levels of a superconducting transmon qubit. *Phys. Rev. Lett.* **114**, 010501 (2015).
76. Kapit, E. Hardware-efficient and fully autonomous quantum error correction in superconducting circuits. *Phys. Rev. Lett.* **116**, 150501 (2016).
77. Takita, M. *et al.* Demonstration of weight-four parity measurements in the surface code architecture. *Phys. Rev. Lett.* **117**, 210505 (2016).
78. Johansson, J. R., Nation, P. D. & Nori, F. Qutip: An open-source python framework for the dynamics of open quantum systems. *Computer Physics Communications* **183**, 1760–1772 (2012).

Acknowledgements

We thank W. D. Oliver, S. Gustavsson, and M. Kjaergaard from the Engineering Quantum Systems Group at MIT for their kind hospitality and for extended discussion on superconducting circuits. This work was supported by the Carlsberg Foundation and the Danish Council for Independent Research under the DFF Sapere Aude program.

Author Contributions

The circuit was designed by L.B.K. and N.J.S.L., and analyzed by L.B.K. and T.B. The numerical calculations were performed by T.B. with suggestions from D.P., C.K.A., N.J.S.L. and N.T.Z. The initial draft of the paper was written by T.B., D.P. and N.T.Z. All authors contributed to the revisions that lead to the final version.

Additional Information

Supplementary information accompanies this paper at <https://doi.org/10.1038/s41598-019-49657-1>.

Competing Interests: The authors declare no competing interests.

Publisher's note Springer Nature remains neutral with regard to jurisdictional claims in published maps and institutional affiliations.



Open Access This article is licensed under a Creative Commons Attribution 4.0 International License, which permits use, sharing, adaptation, distribution and reproduction in any medium or format, as long as you give appropriate credit to the original author(s) and the source, provide a link to the Creative Commons license, and indicate if changes were made. The images or other third party material in this article are included in the article's Creative Commons license, unless indicated otherwise in a credit line to the material. If material is not included in the article's Creative Commons license and your intended use is not permitted by statutory regulation or exceeds the permitted use, you will need to obtain permission directly from the copyright holder. To view a copy of this license, visit <http://creativecommons.org/licenses/by/4.0/>.

© The Author(s) 2019